frontiers | Frontiers in Chemistry

TYPE Original Research
PUBLISHED 19 September 2022
DOI 10.3389/fchem.2022.1021358

OPEN ACCESS

EDITED BY
Zhao-Bo Hu,
Jiangxi University of Science and Technology, China

REVIEWED BY
Xing-Cai Huang,
Yancheng Teachers University, China
Jing Ru,
Liaocheng University, China

*CORRESPONDENCE
Feng Gao,
gf2016@jsnu.edu.cn
Jing-Yuan Ge,
gejingyuan90@126.com

SPECIALTY SECTION
This article was submitted to Inorganic Chemistry, a section of the journal Frontiers in Chemistry

RECEIVED 17 August 2022
ACCEPTED 05 September 2022
PUBLISHED 19 September 2022

CITATION
Sheng Y, Jiang Y-J, Cheng Z-H, Liu R-C, Ge J-Y and Gao F (2022), Syntheses, structures, and magnetic properties of acetate-bridged lanthanide complexes based on a tripodal oxygen ligand. *Front. Chem.* 10:1021358. doi: 10.3389/fchem.2022.1021358

Syntheses, structures, and magnetic properties of acetate-bridged lanthanide complexes based on a tripodal oxygen ligand

Yu Sheng[1], Yu-Jing Jiang[1], Zi-Hang Cheng[1], Ru-Chan Liu[1], Jing-Yuan Ge[2]* and Feng Gao[1]*

[1]School of Chemistry and Materials Science, Jiangsu Normal University, Xuzhou, China, [2]College of Chemistry and Materials Engineering, Wenzhou University, Wenzhou, China

Four homodinuclear lanthanide complexes, $Dy_2(L_{OEt})_2(OAc)_4$ (**1**), $Tb_2(L_{OEt})_2(OAc)_4$ (**2**), $Ho_2(L_{OEt})_2(OAc)_4$ (**3**), and $Gd_2(L_{OEt})_2(OAc)_4$ (**4**), have been synthesized and characterized based on a tripodal oxygen ligand Na [(η^5-C_5H_5)Co(P(O)(OC_2H_5)$_2$)$_3$] (NaL_{OEt}). Structural analyses show that the acetate anions bridge two symmetry-related Ln^{3+} ions in the μ_2:η^1:η^1 and μ_2:η^1:η^2 coordination patterns, and each lanthanide (III) ion owns a twisted square antiprism (SAPR) conformation. Static magnetic measurements reveal the weak intramolecular ferromagnetic interaction between dysprosium (III) ions in **1** and antiferromagnetic Ln^{3+}···Ln^{3+} couplings in the other three complexes. Through the analysis of the ligand-field effect and magnetic anisotropy axis orientation, the reasons for the lack of dynamic magnetic behavior in **1** were identified.

KEYWORDS

lanthanide complexes, ligand-field effect, single-molecule magnets, magnetic properties, magnetic interactions

Introduction

As novel nano-molecular magnetic materials, single-molecule magnets (SMMs), showing slow relaxation of magnetization, have attracted widespread interest in both theoretical and applied research areas because of their intriguing structures and specific physical/chemical properties (Leuenberger and Loss, 2001; Bogani and Wernsdorfer, 2008; Troiani and Affronte, 2011; Li J et al., 2021). It has been found that the introduction of paramagnetic lanthanide ions with larger magnetic anisotropy and stronger spin-orbit coupling is an effective approach to construct promising SMMs.

So far, many high-performance mononuclear lanthanide-based SMMs, also named single-ion magnets (SIMs), have been reported (Liu et al., 2018; Zhu et al., 2019; Parmar et al., 2021; Sutter et al., 2022). The studies revealed that a

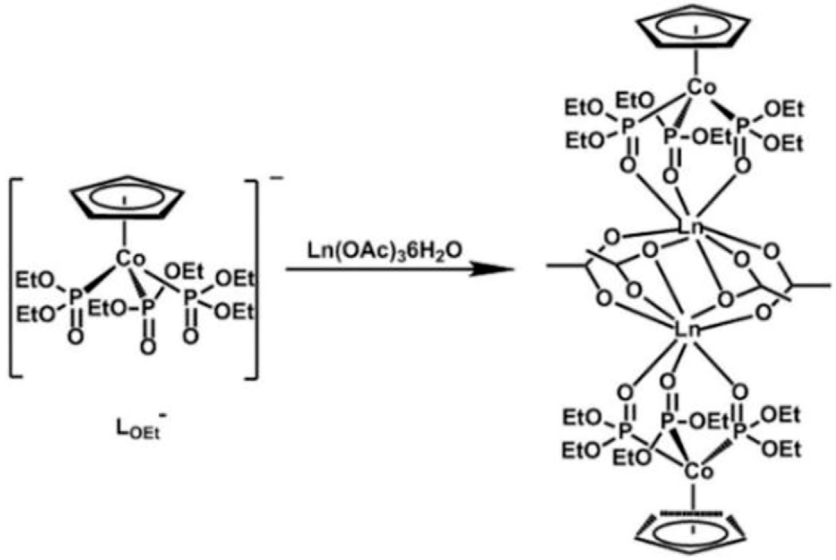

SCHEME 1
Synthetic process of target complexes Ln_2 $(L_{OEt})_2(OAc)_4$ (Ln = Dy (**1**), Tb (**2**), Ho (**3**), and Gd (**4**)).

suitable crystal-field environment with specific symmetry around lanthanide spin centers, such as D_{4d} (Ishikawa et al., 2003; Bala et al., 2019; Zhuo et al., 2021), D_{4h} (Ding et al., 2021; Thomas-Hargreaves et al., 2021), D_{5h} (Chen et al., 2016; Ding et al., 2022; Sutter et al., 2022), D_{6h} (Canaj et al., 2019; Li et al., 2019; Zhu et al., 2021), and C_{∞} (Goodwin et al., 2017; Guo et al., 2017; Guo et al., 2018), usually leads to a remarkable single-ion magnetic anisotropy and slow magnetic relaxation behavior.

For Ln-SIMs, it is convenient to investigate the relationship between the ligand-field effect, uniaxial magnetic anisotropy, and magnetic relaxation processes. However, some factors, e.g., the higher coordination number and relatively low axisymmetric tendency of lanthanide ions and the common quantum tunneling of magnetization (QTM) effect in SIMs, still maintain a certain level of challenge for molecular design.

As an alternative, the research on polynuclear lanthanide-based SMMs, especially simple dinuclear lanthanide systems, provides a broader space for suppressing QTM and fine-tuning the dynamic magnetic behaviors by introducing intramolecular magnetic couplings (Morita et al., 2018; Gao et al., 2019; Goodwin, 2020; Gould et al., 2020; Meng et al., 2020; Li X et al., 2021; Xu et al., 2021).

Many reports on dinuclear Ln-SMMs have shown that the effective regulation of local symmetry around spin carriers, magnetic anisotropy axis orientation, and the strength and nature of paramagnetic $Ln^{3+}\cdots Ln^{3+}$ magnetic interactions through choosing appropriate ligands is still the focus of current research. Therefore, four new acetate-bridged dinuclear lanthanide complexes Dy_2 $(L_{OEt})_2(OAc)_4$ (**1**), Tb_2 $(L_{OEt})_2(OAc)_4$ (**2**), $Ho_2(L_{OEt})_2(OAc)_4$ (**3**), and Gd_2 $(L_{OEt})_2(OAc)_4$ (**4**) were designed and prepared in this study by virtue of the chelation coordination feature of a tripodal oxygen ligand Na $[(\eta^5\text{-}C_5H_5)Co(P(O)(OC_2H_5)_2)_3]$ (NaL_{OEt}) and the variable bridge modes of acetate anion (Scheme 1). Their crystal structures and magnetic properties were also significantly investigated.

Experimental sections

Preparation of Dy_2 $(L_{OEt})_2(OAc)_4$ (1)

For the preparation, 27.8 mg (0.062 mmol) $Dy(OAc)_3{\cdot}6H_2O$ and 35.6 mg (0.062 mmol) tripodal ligand NaL_{OEt} were dissolved in 8 ml of methanol and 5 ml of acetone. The resultant solution was treated for 10 h at 90°C. After about 6 days, suitable yellow crystals can be produced by evaporating the clear mother solution at room temperature (yield = 52%, based on NaL_{OEt}). Main IR data (cm^{-1}): 2977(m), 1625(s), 1447(m), 1416(m), 1142(s), 1038(s), 932(m), 832(m), 771(m), 722(m), and 583(m). Anal. Calcd for $C_{42}H_{82}Co_2Dy_2O_{26}P_6$ (%): C, 30.91; H, 5.07. Found: C, 31.10; H, 5.23. UV-Vis (λ_{max}/nm with log (ε/dm^3 mol^{-1} cm^{-1})): 245(4.77) and 335(3.92).

Preparation of Tb_2 $(L_{OEt})_2(OAc)_4$ (2)

The preparation of Tb_2 $(L_{OEt})_2(OAc)_4$ (**2**) followed the same procedure as (**1**), using 27.5 mg (0.062 mmol) $Tb(OAc)_3{\cdot}6H_2O$. Similar yellow crystals can be produced (yield = 45%, based on NaL_{OEt}). Main IR data (cm^{-1}): 2977(m), 1621(s), 1442(m), 1414(m), 1141(s), 1038(s), 932(m), 832(m), 771(m), 721(m), and 582(m). Anal. Calcd for $C_{42}H_{82}Co_2Tb_2O_{26}P_6$ (%): C, 31.05; H, 5.09. Found: C, 31.23; H, 5.26. UV-Vis (λ_{max}/nm with log (ε/dm^3 mol^{-1} cm^{-1})): 244(4.78) and 335(3.91).

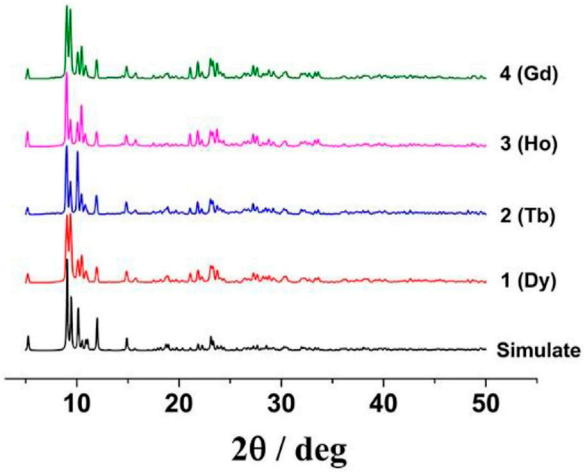

FIGURE 1
Experimental and simulated PXRD patterns of all complexes.

Preparation of $Ho_2(L_{OEt})_2(OAc)_4$ (3)

The preparation of $Ho_2(L_{OEt})_2(OAc)_4$ (**3**) followed the same procedure as (**1**), using 27.9 mg (0.062 mmol) $Ho(OAc)_3{\cdot}6H_2O$. Similar yellow crystals can be produced (yield = 46%, based on NaL_{OEt}). Main IR data (cm^{-1}): 2978(m), 1623(s), 1445(m), 1414(m), 1141(s), 1038(s), 933(m), 832(m), 770(m), 722(m), and 582(m). Anal. Calcd for $C_{42}H_{82}Co_2Ho_2O_{26}P_6$ (%): C, 30.82; H, 5.05. Found: C, 31.01; H, 5.25. UV-Vis (λ_{max}/nm with log (ε/dm^3 mol^{-1} cm^{-1})): 244(4.77) and 335(3.90).

Preparation of Gd_2 $(L_{OEt})_2(OAc)_4$ (4)

The preparation of Gd_2 $(L_{OEt})_2(OAc)_4$ (**4**) followed the same procedure as (**1**), using 27.4 mg (0.062 mmol) $Gd(OAc)_3{\cdot}6H_2O$. Similar yellow crystals can be produced (yield = 48%, based on NaL_{OEt}). Main IR data (cm^{-1}): 2977(m), 1624(s), 1446(m), 1415(m), 1142(s), 1039(s), 932(m), 831(m), 771(m), 722(m), and 582(m). Anal. Calcd for $C_{42}H_{82}Co_2Gd_2O_{26}P_6$ (%): C, 31.11; H, 5.10. Found: C, 31.30; H, 5.28. UV-Vis (λ_{max}/nm with log (ε/dm^3 mol^{-1} cm^{-1})): 243(4.77) and 334(3.89).

Result and discussion

As mentioned earlier, the organometallic tripodal oxygen ligand NaL_{OEt} is an ideal building block to encapsulate metal cores with its oxygen-based tridentate coordination sites (Gao et al., 2014; Lim et al., 2016; Van Raden et al., 2022). As a result, target lanthanide complexes were synthesized by a one-step

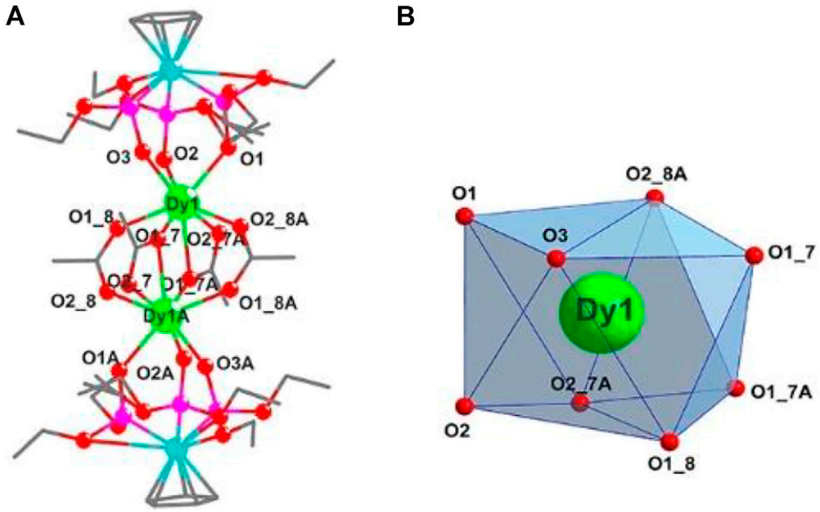

FIGURE 2
(A) Molecular structure diagram of **1** (Dy, green; Co, aqua; O, red; P, pink; and C, gray). The H atoms are omitted for clarity. **(B)** Coordination polyhedron of the $Dy1^{3+}$ ion.

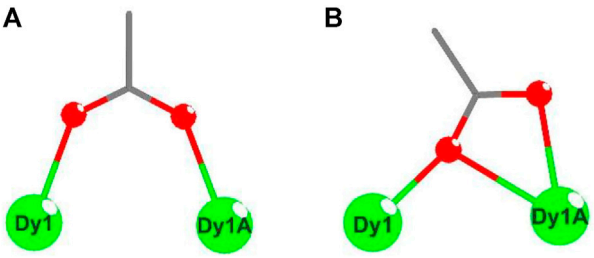

FIGURE 3
Two coordination patterns μ_2:η^1:η^1 **(A)** and μ_2:η^1:η^2 **(B)** of acetate groups in **1**.

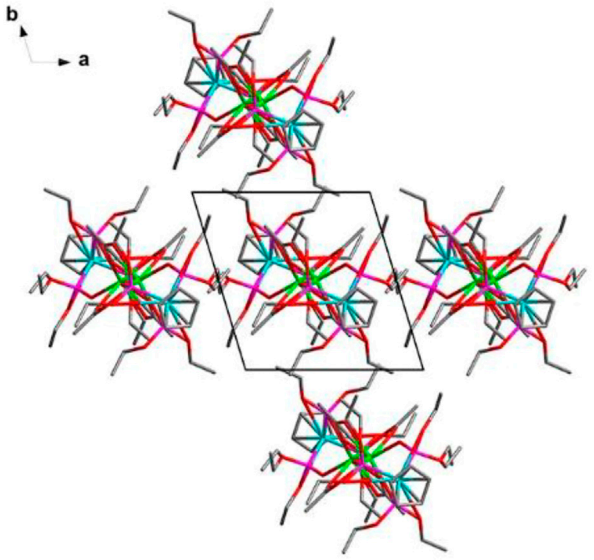

FIGURE 4
Molecular structure packing diagram along the *c*-axis of **1**.

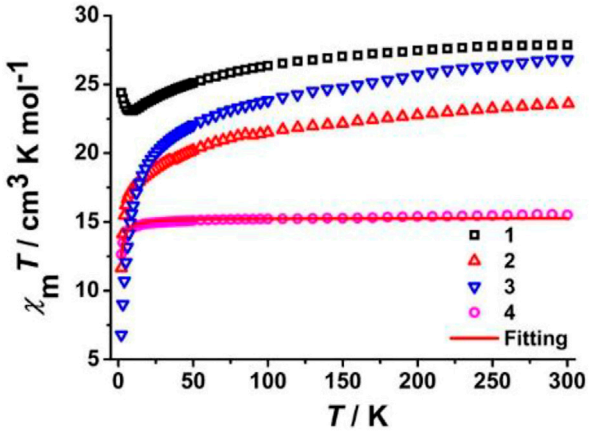

FIGURE 5
Temperature-dependent $\chi_M T$ plots under H_{dc} = 1 kOe of all prepared complexes. The red curve is the fitting result of the experimental $\chi_M T$ products of **4**.

reaction of various lanthanide acetate hydrates with NaL_{OEt}. Satisfactory crystals for X-ray crystallography can be obtained by evaporating the mixed solution. These air-stable complexes are readily soluble in acetonitrile, acetone, dichloromethane, and methanol. Detailed characterization has been performed by IR spectra, elemental analysis, UV-Vis absorption spectra (Supplementary Figure S1), and magnetic measurements.

Purity analysis

Powder X-ray diffraction (PXRD) experiment data were measured at room temperature to verify the phase purity of crystal samples. The main experimental peaks match well with the simulated PXRD patterns according to the X-ray crystal data on the respective complexes (Figure 1), confirming the good purity of the prepared products.

Crystal structure description

These electrically neutral complexes crystallize in the triclinic crystal system ($P\bar{1}$ space group), and each asymmetric unit contains one Ln^{3+} ion, one tripodal anionic ligand $[L_{OEt}]^-$, and two acetate anions (Figure 2 and Supplementary Figures S2–S4). Related crystallographic parameters are listed in Supplementary Table S1 with CCDC numbers 2182586 (1), 2182587 (2), 2182588 (3), and 2182589 (4). Some main bond length and bond angle data are presented in Supplementary Table S2. Because they are crystallographically isostructural, only the molecular structure of **1** is fully described as a representative. In Figure 2A, the paramagnetic $Dy1^{3+}$ ion is coordinated through eight oxygen atoms (O1, O2, and O3 from tripodal anionic $[L_{OEt}]^-$, O1_7, O1_8, O1_7A, O2_7A, and O2_8A from acetate anions, respectively). These Dy-O bond lengths range between 2.311 (2) and 2.537 (2) Å. The tripodal anionic $[L_{OEt}]^-$ situates above the dysprosium (III) ion, and the diamagnetic cobalt (III) ion is surrounded by three phosphorus atoms and a cyclopentadienyl ring. The acetate anions use two different coordination patterns, μ_2:η^1:η^1 (Figure 3A) and μ_2:η^1:η^2 (Figure 3B), to bridge two symmetry-related dysprosium (III) ions with an intramolecular $Dy1^{3+}$···$Dy1A^{3+}$ distance of 3.915 (8) Å. The continuous shape measurement (CShM) method by *SHAPE* analysis (Alvarez et al., 2005) was performed to determine the precise geometry of lanthanide centers (Supplementary Table S3). The eight-coordinated paramagnetic dysprosium (III) ion in **1** has a twisted square

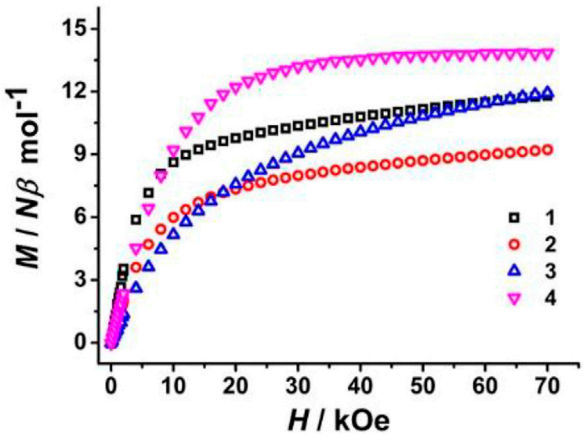

FIGURE 6
Magnetic field-dependent magnetization plots of all prepared complexes.

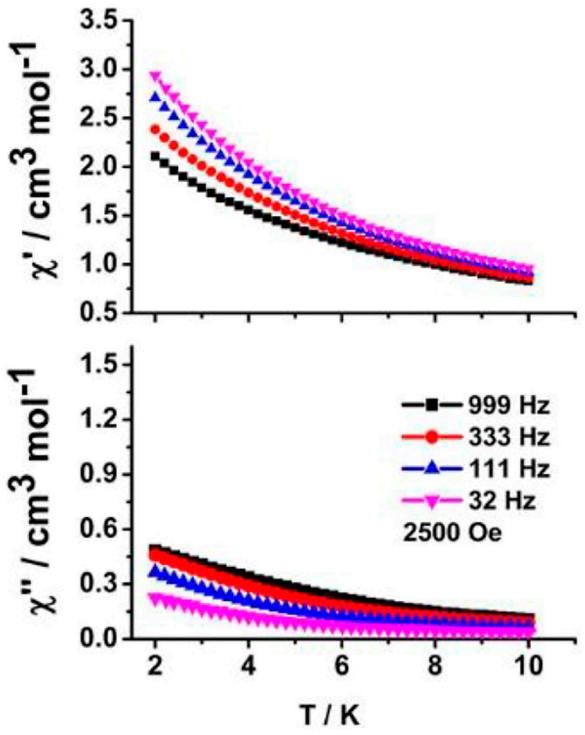

FIGURE 7
Temperature-dependent in-phase (χ′) (up) and out-of-phase (χ″) (down) ac susceptibility curves under H_{dc} = 2,500 Oe of **1**.

antiprism (SAPR, D_{4d}) conformation (Figure 2B) with calculated CShM value S = 1.619. As shown in the crystal packing diagram of **1** (Figure 4), no special intermolecular interactions can be found with the shortest intermolecular distance between dysprosium (III) ions of 9.844 (3) Å.

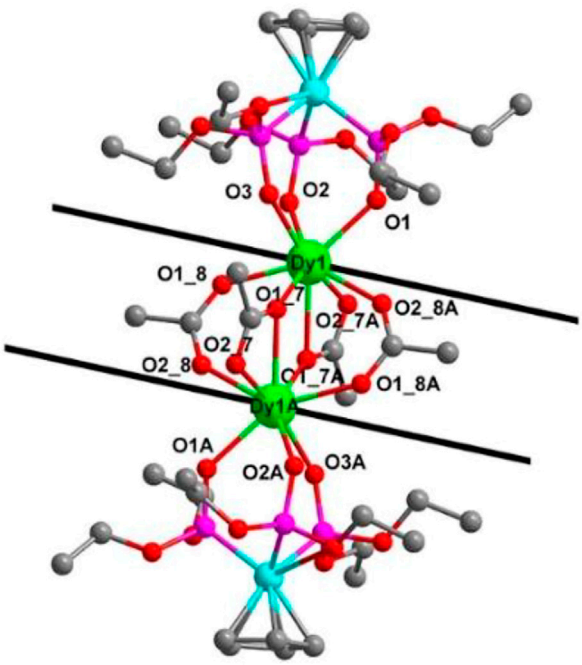

FIGURE 8
Ground state (M_J = ±15/2) magnetic anisotropy axes' direction of dysprosium (III) ion in **1**.

Magnetism investigation

Temperature-dependent direct current (dc) magnetic susceptibility plots ($\chi_M T$ vs. T) are presented in Figure 5, which were collected under H_{dc} = 1 kOe between 2.0 and 300 K. Since the diamagnetic cobalt (III) cations in the system have no effect on magnetic properties, the measured $\chi_M T$ values at 300 K are 27.87 (**1**), 23.60 (**2**), 26.82 (**3**), and 15.51 (**4**) cm^3 K mol^{-1}, comparable to the theoretically calculated results for two isolated paramagnetic lanthanide (III) ions. In high-temperature regions, the $\chi_M T$ products of **1**, **2**, and **3** decrease slowly and reach the respective minimum values of 23.08 (**1**, 9.0 K), 11.65 (**2**, 2.0 K), and 6.81 (**3**, 2.0 K) cm^3 K mol^{-1}, usually caused by antiferromagnetic couplings between adjacent lanthanide (III) ions, and/or depopulation of Ln^{3+} ions excited Stark (M_J) sublevels (Lim et al., 2016; Liu et al., 2016; Li J et al., 2021). Upon lowering the temperature to 2.0 K, the $\chi_M T$ value of **1** rises again to a maximum of 24.40 cm^3 K mol^{-1}, indicating the existence of weak intramolecular ferromagnetic interactions between the paramagnetic dysprosium (III) centers (Gao et al., 2019; Shen et al., 2020; Li X et al., 2021; Liu et al., 2021). In **4**, the $\chi_M T$ values are almost unchanged from 300 to 30.0 K and drop eventually to around 2.0 K to 12.64 cm^3 K mol^{-1}, suggesting the occurrence of antiferromagnetic $Gd^{3+}\cdots Gd^{3+}$ coupling. Subsequently, the isotropic spin Hamiltonian equation $\hat{H} = -2J\hat{S}_{Gd1}\cdot\hat{S}_{Gd1A}$ was applied to fit $\chi_M T$ vs. T data on **2** in order to reveal the nature and strength of the magnetic interaction between gadolinium (III) ions. The calculated

values using the *PHI* program (Chilton et al., 2013a) are $g = 1.98$ and $J = -0.025$ cm^{-1} (the negative J value reveals weak antiferromagnetic interactions between gadolinium (III) ions).

Magnetic field-dependent magnetizations (M vs. H) of all prepared complexes were then measured at 2.0 K under magnetic fields between 0 and 70 kOe, showing that M rises rapidly below about 15 kOe and then increases slowly in the high-magnetic field region (Figure 6). The M values at H_{dc} = 70 kOe are 11.80 Nβ for **1**, 9.22 Nβ for **2**, and 11.94 Nβ for **3**. Such deviation from their respective theoretical saturation M values is ascribed to crystal field-induced low-excited states and significant magnetic anisotropy (Hutchings et al., 2014; Yang et al., 2014; Gao et al., 2019), while the maximum M value of **4** (13.84 Nβ) is consistent with the saturation value of 14.0 Nβ for two noninteracting gadolinium (III) ions.

Alternative current (ac) magnetic experiments were measured to study its dynamic magnetic behavior. Unfortunately, no obvious temperature-dependent out-of-phase (χ") susceptibility signal peaks at the high frequency of 999 Hz were shown under H_{dc} = 0 Oe for **1** containing anisotropic Kramer dysprosium (III) ions (Supplementary Figure S5), possibly originating from the effect of stronger QTM. As a further investigation, the dc magnetic field of 2,500 Oe was employed. The expected χ" signal peaks were still unable to be observed (Figure 7). We think there are two main reasons for the lack of SMM behavior in **1**. On the one hand, the relatively larger distortion from the ideal D_{4d} geometry around the dysprosium (III) center (higher calculated CShM value S_{SAPR} = 1.619) may lead to the weaker ligand-field effect and uniaxial magnetic anisotropy. On the other hand, electrostatic calculation by means of the *MAGELLAN* program (Chilton et al., 2013b) was used to judge the direction of dysprosium (III) ion's ground state ($M_J = \pm 15/2$) magnetic anisotropy axis (Figure 8). The result shows that the two magnetic axes are parallel to each other in a centrosymmetric molecule, and the angle between the magnetic axis of the $Dy1^{3+}$ ion and the unit vector linking two dysprosium (III) ions ($Dy1^{3+}$ and $Dy1A^{3+}$) is 86.6°. Furthermore, as an important structural parameter affecting the ligand field strength, the Dy1-O2 bond length is 2.311 (2) Å, which is the shortest among those other Dy-O bond lengths in the twisted SAPR polyhedron. The magnetic axis of the $Dy1^{3+}$ ion is aligned along the shortest Dy1-O2 bond with an included angle of 58.4°. The above-mentioned two large angular deviations confirm that such a weak ligand field in this system is not conductive to activating the magnetic relaxation process.

For complexes **2** and **3** containing anisotropic non-Kramer lanthanide (III) ions, the χ" signals were also very weak at the frequency of 999 Hz under H_{dc} = 0 Oe and H_{dc} = 2,500 Oe, respectively (Supplementary Figures S6, S7), which is raised by their fast magnetization relaxation behavior in such a weak ligand field environment.

Conclusion

In this work, we reported four acetate-bridged homodinuclear lanthanide complexes based on a tripodal oxygen ligand NaL_{OEt}. Structural analyses show acetate anions bridge two symmetry-related Ln^{3+} ions in the μ_2:η^1:η^1 and μ_2:η^1:η^2 coordination patterns, and each lanthanide ion owns a twisted SAPR conformation. Magnetic analyses reveal the weak intramolecular ferromagnetic interaction between dysprosium (III) ions in **1** and antiferromagnetic $Ln^{3+}\cdots Ln^{3+}$ coupling in the other complexes. The weaker ligand-field effect caused by the larger distorted geometry and the deviation of the magnetic anisotropy axis orientation with a specific lanthanide–ligand coordination bond leads to the lack of SMM behavior.

Although the expected SMM behaviors could not be found in this system, these well-known factors, including the effective suppression of QTM, regulation of $Ln^{3+}\cdots Ln^{3+}$ magnetic interactions, and construction of reasonable crystal field symmetry, still remain important for affecting the slow magnetic relaxation behaviors of SMMs. Further efforts to design, synthesize, and study novel molecular magnetic materials are in progress in our group.

Data availability statement

The datasets presented in this study can be found in online repositories. The names of the repository/repositories and accession number(s) can be found in the article/ Supplementary Material.

Author contributions

Idea and methodology were conceived by YS, Y-JJ, and FG. Synthesis and crystals grown were performed by YS, Y-JJ, Z-HC, and R-CL. General characterization and crystal structural analysis were performed by YS, Y-JJ, Z-HC, J-YG, and FG. Magnetic testing and data analysis were performed by YS, J-YG, and FG. The manuscript was drafted and edited by YS, Y-JJ, J-YG, and FG. All authors have given approval to the manuscript.

Funding

This work was supported by the National Natural Science Foundation of China (No. 21401085) and the Priority Academic Program Development (PAPD) of Jiangsu Higher Education Institutions.

Conflict of interest

The authors declare that the research was conducted in the absence of any commercial or financial relationships that could be construed as a potential conflict of interest.

Publisher's note

All claims expressed in this article are solely those of the authors and do not necessarily represent those of their affiliated organizations, or those of the publisher, the editors, and the reviewers. Any product that may be evaluated in this article, or claim that may be made by its manufacturer, is not guaranteed or endorsed by the publisher.

Supplementary material

The Supplementary Material for this article can be found online at: https://www.frontiersin.org/articles/10.3389/fchem.2022.1021358/full#supplementary-material

References

Alvarez, S., Alemany, P., Casanova, D., Cirera, J., Llunell, M., and Avnir, D. (2005). Shape maps and polyhedral interconversion paths in transition metal chemistry. *Coord. Chem. Rev.* 249 (17-18), 1693–1708. doi:10.1016/j.ccr.2005.03.031

Bala, S., Huang, G. Z., Ruan, Z. Y., Wu, S. G., Liu, Y., Wang, L. F., et al. (2019). A square antiprism dysprosium single-ion magnet with an energy barrier over 900 K. *Chem. Commun.* 55 (67), 9939–9942. doi:10.1039/c9cc05135j

Bogani, L., and Wernsdorfer, W. (2008). Molecular spintronics using single-molecule magnets. *Nat. Mat.* 7 (3), 179–186. doi:10.1038/nmat2133

Canaj, A. B., Dey, S., Martí, E. R., Wilson, C., Rajaraman, G., and Murrie, M. (2019). Insight into D_{6h} symmetry: Targeting strong axiality in stable dysprosium(III) hexagonal bipyramidal single-ion magnets. *Angew. Chem. Int. Ed.* 58 (40), 14146–14151. doi:10.1002/anie.201907686

Chen, Y. C., Liu, J. L., Ungur, L., Liu, J., Li, Q. W., Wang, L. F., et al. (2016). Symmetry-supported magnetic blocking at 20 K in pentagonal bipyramidal Dy(III) single-ion magnets. *J. Am. Chem. Soc.* 138 (8), 2829–2837. doi:10.1021/jacs.5b13584

Chilton, N. F., Anderson, R. P., Turner, L. D., Soncini, A., and Murray, K. S. (2013a). Phi: A powerful new program for the analysis of anisotropic monomeric and exchange-coupled polynuclear d- and f-block complexes. *J. Comput. Chem.* 34 (13), 1164–1175. doi:10.1002/jcc.23234

Chilton, N. F., Collison, D., McInnes, E. J. L., Winpenny, R. E. P., and Soncini, A. (2013b). An electrostatic model for the determination of magnetic anisotropy in dysprosium complexes. *Nat. Commun.* 4, 2551. doi:10.1038/ncomms3551

Ding, X., Luo, Q., Zhai, Y., Zhang, X., Lv, Y., Zhang, X., et al. (2022). Rigid dysprosium(III) single-molecule magnets exhibit preserved superparamagnetism in solution. *Chin. J. Chem.* 40 (5), 563–570. doi:10.1002/cjoc.202100722

Ding, X. L., Zhai, Y. Q., Han, T., Chen, W. P., Ding, Y. S., and Zheng, Y. Z. (2021). A local D_{4h} symmetric dysprosium(III) single-molecule magnet with an energy barrier exceeding 2000 K. *Chem. Eur. J.* 27 (8), 2623–2627. doi:10.1002/chem.202003931

Gao, F., Cui, L., Song, Y., Li, Y. Z., and Zuo, J. L. (2014). Calix[4]arene-supported mononuclear lanthanide single-molecule magnet. *Inorg. Chem.* 53 (1), 562–567. doi:10.1021/ic4026624

Gao, F., Wang, L., Zhu, G. Z., Liu, Y. H., Yang, H., Li, X., et al. (2019). Controllable syntheses and magnetic properties of novel homoleptic triple-decker lanthanide complexes. *Dalton Trans.* 48 (35), 13360–13368. doi:10.1039/c9dt02565k

Goodwin, C. A. P. (2020). Blocking like it's hot: A synthetic chemists' path to high-temperature lanthanide single molecule magnets. *Dalton Trans.* 49 (41), 14320–14337. doi:10.1039/d0dt01904f

Goodwin, C. A. P., Ortu, F., Reta, D., Chilton, N. F., and Mills, D. P. (2017). Molecular magnetic hysteresis at 60 kelvin in dysprosocenium. *Nature* 548 (7668), 439–442. doi:10.1038/nature23447

Gould, C. A., Mu, E., Vieru, V., Darago, L. E., Chakarawet, K., Gonzalez, M. I., et al. (2020). Substituent effects on exchange coupling and magnetic relaxation in 2, 2'-bipyrimidine radical-bridged dilanthanide complexes. *J. Am. Chem. Soc.* 142 (50), 21197–21209. doi:10.1021/jacs.0c10612

Guo, F. S., Day, B. M., Chen, Y. C., Tong, M. L., Mansikkamäki, A., and Layfield, R. A. (2017). A dysprosium metallocene single-molecule magnet functioning at the axial limit. *Angew. Chem. Int. Ed.* 56 (38), 11445–11449. doi:10.1002/anie.201705426

Guo, F. S., Day, B. M., Chen, Y. C., Tong, M. L., Mansikkamäki, A., and Layfield, R. A. (2018). Magnetic hysteresis up to 80 kelvin in a dysprosium metallocene single-molecule magnet. *Science* 362 (6421), 1400–1403. doi:10.1126/science.aav0652

Hutchings, A. J., Habib, F., Holmberg, R. J., Korobkov, I., and Murugesu, M. (2014). Structural rearrangement through lanthanide contraction in dinuclear complexes. *Inorg. Chem.* 53 (4), 2102–2112. doi:10.1021/ic402682r

Ishikawa, N., Sugita, M., Ishikawa, T., Koshihara, S., and Kaizu, Y. (2003). Lanthanide double-decker complexes functioning as magnets at the single-molecular level. *J. Am. Chem. Soc.* 125 (29), 8694–8695. doi:10.1021/ja029629n

Leuenberger, M. N., and Loss, D. (2001). Quantum computing in molecular magnets. *Nature* 410 (6830), 789–793. doi:10.1038/35071024

Li, J., Xiong, S.-J., Li, C., Jin, B., Zhang, Y.-Q., Jiang, S.-D., et al. (2021). Manipulation of molecular qubits by isotope effect on spin dynamics. *CCS Chem.* 3 (9), 2548–2556. doi:10.31635/ccschem.020.202000384

Li, X., Liu, Y. H., Zhu, G. Z., Yang, F. L., and Gao, F. (2021). Successive syntheses and magnetic properties of homodinuclear lanthanide macrocyclic complexes. *Dalton Trans.* 50 (35), 12215–12225. doi:10.1039/d1dt01514a

Li, Z. H., Zhai, Y. Q., Chen, W. P., Ding, Y. S., and Zheng, Y. Z. (2019). Air-stable hexagonal bipyramidal dysprosium(III) single-ion magnets with nearly perfect D_{6h} local symmetry. *Chem. Eur. J.* 25 (71), 16219–16224. doi:10.1002/chem.201904325

Lim, K. S., Baldoví, J. J., Lee, W. R., Song, J. H., Yoon, S. W., Suh, B. J., et al. (2016). Switching of slow magnetic relaxation dynamics in mononuclear dysprosium(III) compounds with charge density. *Inorg. Chem.* 55 (11), 5398–5404. doi:10.1021/acs.inorgchem.6b00410

Liu, C. M., Sun, R., Wang, B. W., Wu, F., Hao, X., and Shen, Z. (2021). Homochiral ferromagnetic coupling Dy_2 single-molecule magnets with strong magneto-optical faraday effects at room temperature. *Inorg. Chem.* 60 (16), 12039–12048. doi:10.1021/acs.inorgchem.1c01218

Liu, J., Chen, Y. C., Liu, J. L., Vieru, V., Ungur, L., Jia, J. H., et al. (2016). A stable pentagonal bipyramidal Dy(III) single-ion magnet with a record magnetization reversal barrier over 1000 K. *J. Am. Chem. Soc.* 138 (16), 5441–5450. doi:10.1021/jacs.6b02638

Liu, J. L., Chen, Y. C., and Tong, M. L. (2018). Symmetry strategies for high performance lanthanide-based single-molecule magnets. *Chem. Soc. Rev.* 47 (7), 2431–2453. doi:10.1039/c7cs00266a

Meng, Y. S., Qiao, Y. S., Yang, M. W., Xiong, J., Liu, T., Zhang, Y. Q., et al. (2020). Weak exchange coupling effects leading to fast magnetic relaxations in a trinuclear dysprosium single-molecule magnet. *Inorg. Chem. Front.* 7 (2), 447–454. doi:10.1039/c9qi01252d

Morita, T., Damjanovic, M., Katoh, K., Kitagawa, Y., Yasuda, N., Lan, Y., et al. (2018). Comparison of the magnetic anisotropy and spin relaxation phenomenon of dinuclear terbium(III) phthalocyaninato single-molecule magnets using the geometric spin arrangement. *J. Am. Chem. Soc.* 140 (8), 2995–3007. doi:10.1021/jacs.7b12667

Parmar, V. S., Mills, D. P., and Winpenny, R. E. P. (2021). Mononuclear dysprosium alkoxide and aryloxide single-molecule magnets. *Chem. Eur. J.* 27 (28), 7625–7645. doi:10.1002/chem.202100085

Shen, F. X., Pramanik, K., Brandao, P., Zhang, Y. Q., Jana, N. C., Wang, X. Y., et al. (2020). Macrocycle supported dimetallic lanthanide complexes with slow magnetic relaxation in Dy_2 analogues. *Dalton Trans.* 49 (40), 14169–14179. doi:10.1039/d0dt02778b

Sutter, J. P., Béreau, V., Jubault, V., Bretosh, K., Pichon, C., and Duhayon, C. (2022). Magnetic anisotropy of transition metal and lanthanide ions in pentagonal bipyramidal geometry. *Chem. Soc. Rev.* 51 (8), 3280–3313. doi:10.1039/d2cs00028h

Thomas-Hargreaves, L. R., Hunger, D., Kern, M., Wooles, A. J., van Slageren, J., Chilton, N. F., et al. (2021). Insights into D_{4h}@metal-symmetry single-molecule magnetism: The case of a dysprosium-bis(boryloxide) complex. *Chem. Commun.* 57 (6), 733–736. doi:10.1039/d0cc07446b

Troiani, F., and Affronte, M. (2011). Molecular spins for quantum information technologies. *Chem. Soc. Rev.* 40 (6), 3119–3129. doi:10.1039/c0cs00158a

Van Raden, J. M., Alexandropoulos, D. I., Slota, M., Sopp, S., Matsuno, T., Thompson, A. L., et al. (2022). Singly and triply linked magnetic porphyrin lanthanide arrays. *J. Am. Chem. Soc.* 144 (19), 8693–8706. doi:10.1021/jacs.2c02084

Xu, S. M., An, Z. W., Zhang, W., Zhang, Y. Q., and Yao, M. X. (2021). Ligand field and anion-driven structures and magnetic properties of dysprosium complexes. *CrystEngComm* 23 (15), 2825–2834. doi:10.1039/d1ce00115a

Yang, F., Zhou, Q., Zeng, G., Li, G., Gao, L., Shi, Z., et al. (2014). Anion effects on the structures and magnetic properties of binuclear lanthanide single-molecule magnets. *Dalton Trans.* 43 (3), 1238–1245. doi:10.1039/c3dt52634h

Zhu, Z., Guo, M., Li, X. L., and Tang, J. (2019). Molecular magnetism of lanthanide: Advances and perspectives. *Coord. Chem. Rev.* 378, 350–364. doi:10.1016/j.ccr.2017.10.030

Zhu, Z., Zhao, C., Feng, T., Liu, X., Ying, X., Li, X. L., et al. (2021). Air-stable chiral single-molecule magnets with record anisotropy barrier exceeding 1800 K. *J. Am. Chem. Soc.* 143 (27), 10077–10082. doi:10.1021/jacs.1c05279

Zhuo, W., Tian, Y. M., Chen, P., Sun, W. B., Wang, B. W., and Gao, S. (2021). A series of counter cation-dependent tetra β-diketonate mononuclear lanthanide(III) single-molecule magnets and immobilization on pre-functionalised gan substrates by anion exchange reaction. *J. Mat. Chem. C* 9 (21), 6911–6922. doi:10.1039/d1tc01263k